Theoretical Study of Intramolecular Proton Transfer Reactions in Some Thiooxalic Acid Derivatives

Eduardo Chamorro,*,†,§ Alejandro Toro-Labbe,‡ and Patricio Fuentealba†

Departamento de Física, Facultad de Ciencias, Universidad de Chile, Casilla 653, Santiago, Chile, and Departamento de Química-Física, Facultad de Química, Pontificia Universidad Católica de Chile, Casilla 306, Santiago 22, Chile

Received: November 26, 2001; In Final Form: February 5, 2002

The intramolecular proton-transfer reactions in some thiooxalic acid derivatives HY−C(═O)−C(═S)−XH, (1) X═O, Y═O; (2) X═O, Y═S; (3) X═S, Y═S, have been studied in the gas-phase at the B3LYP/6-311+G(d,p) level of theory. Reactions are shown to proceed via a two step mechanism more than through single concerted interconversions. Four-membered transition states are involved along the oxygen to oxygen, sulfur to oxygen, and sulfur to sulfur, single proton-transfer processes. The double proton-transfer reaction in these systems is a competitive and coupled process with the conformational rearrangement through the central C−C bond. Reaction mechanisms have been discussed in terms of global and local chemical reactivity descriptors. The electronic nature of the transferred hydrogen has been explicitly examined using the topological analysis of the electron localization function (ELF). Ion-pair like transition structures with charge separations of 0.48e, 0.42e, and 0.18e have been found for the oxygen to oxygen, sulfur to oxygen, and sulfur to sulfur proton-transfer reactions, respectively, in these type of proton-transfer processes.

Introduction

Proton-transfer reactions are one of the most important processes in chemistry and biochemistry. The understanding of several issues of reactivity compelling such reactions have been the subject of extensive research from both experimental and theoretical viewpoints.[1−6] The carboxyl group and their poly thio derivatives are among the most important and versatile functional groups in chemistry. In particular, oxalate and its thio-homologues have important ligand properties for coordination chemistry.[7−9] The literature concerning the gas-phase acidities of formic acid and its silicon and sulfur derivatives has been recently revised by Remko.[10] Surprinsingly, more information related to the nature of simple proton transfer in these specific systems has not been found although must be mentioned that studies of tautomerism in thiocarboxylic acids has been previously reported.[11,12] In this work, we have carried out a theoretical study of the intramolecular proton-transfer reactions in the monothiooxalic (1), 1,2-dithiooxalic (2), and trithiooxalic (3) derivatives, i.e., the HY−C(═O)−C(═S)−XH systems (**1**: X═O, Y═O; **2**: X═O, Y═S; **3**: X═S, Y═S). They could experience proton-transfer reactions as indicated in Figure 1.

Through the pathway 0, this reaction is to be considered as a single concerted interconversion reaction through a five-membered transition state (TS0a) or through a four-membered transition state (TS0b). The two step processes through the pathways 1 and 2 depend on which single proton-transfer reaction, H(Y)→O or H(X)→S, is the determinant process along the complete reaction coordinate. In the absence of both experimental and theoretical studies concerning the mechanism of the intramolecular proton-transfer process in these systems, we have focused on the theoretical study of the reaction pathway scheme as depicted in Figure 1. Our goal is to examine in some

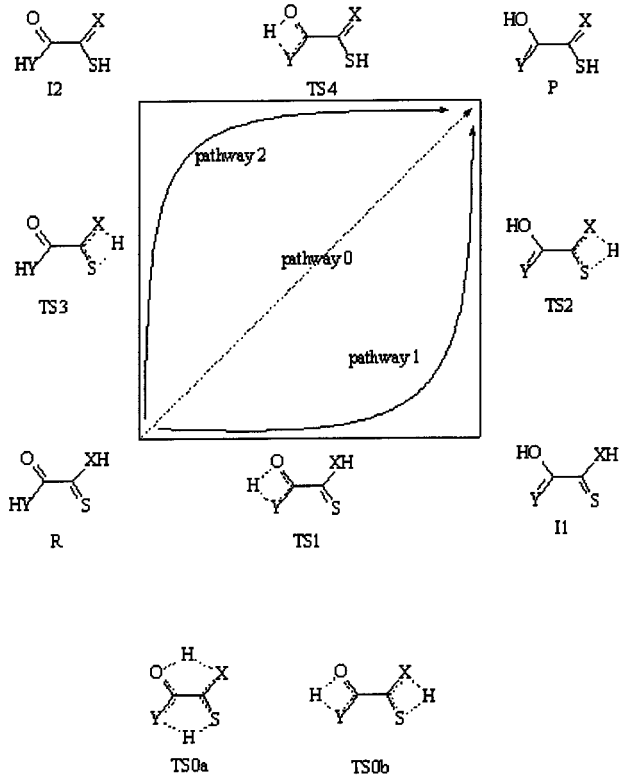

Figure 1. Schematic representation of some possible structures involucred in the intramolecular double proton-transfer reaction mechanism in the thiooxalic acid derivatives: HY−C(═O)−C(═S)−XH systems: (**1**) X═O, Y═O; (**2**) X═O, Y═S; (**3**) X═S, Y═S.

† Departamento de Física, Facultad de Ciencias, Universidad de Chile.
‡ Departamento de Química-Física, Facultad de Química, Pontificia Universidad Católica de Chile.
§ Current address: Facultad de Ecologia y Recursos Naturales, Universidad Nacional Andres Bello, Republica 217, Santiago, Chile.

10.1021/jp0143185 CCC: $22.00
Published on Web 03/19/2002

detail the energetic relationships between the involved species and how the electronic charge rearrangement along the H-transfer path proceed in these systems. The topological analysis of the electron localization function (ELF)[13] have been also employed in order to gain insights about the electronic nature of the transition structures in the oxygen to oxygen, sulfur to oxygen, and sulfur to sulfur proton-transfer reactions implicated in the present study.

Theoretical Background

In the framework of density functional theory (DFT),[14] global descriptors of chemical reactivity correspond to global responses of systems to global perturbations (for instance, changes in the number of electrons N), whereas the external potential $\upsilon(\mathbf{r})$ remains constant. Among such types of indexes, the chemical potential μ,[15,16] chemical hardness η,[17] and softness s[18] can be used as complementary tools in the description of thermodynamic aspects of chemical reactivity. Operational schemes for the calculation of these quantities are based on a finite difference approximation, using the Koopmans' theorem in terms of the frontier HOMO (ϵ_H) and LUMO (ϵ_L) molecular orbital energies.[19] Thus, we have that

$$\mu = \left[\frac{\partial E}{\partial N}\right]_{\upsilon(r)} \approx \frac{1}{2}(\epsilon_H + \epsilon_L) \tag{1}$$

$$\eta = \left[\frac{\partial \mu}{\partial N}\right]_{\upsilon(r)} \approx \frac{1}{2}(\epsilon_L - \epsilon_H) \tag{2}$$

and

$$s = \frac{1}{\eta} \tag{3}$$

These global quantities, as well as the mean polarizability values $\langle\alpha\rangle$, have been found very useful and complementary tools for the description of chemical reactivity in connection with minimum polarizability (MPP)[20] and maximum hardness principles (MHP).[21−26] The $\langle\alpha\rangle$ values can be calculated from the aritmethic average of the corresponding tensor components evaluated using the Sadlej's basis set as it has been recommended[27,28]

$$\langle\alpha\rangle = \frac{1}{3}(\alpha_{xx} + \alpha_{yy} + \alpha_{zz}) \tag{4}$$

In conection with the global ideas of chemical reactivity, the transition structure can be characterized through its intrinsic properties, the energy barrier $\Delta V^{\neq} = [V(TS) - V(R)]$, the activation chemical potential $\Delta\mu^{\neq} = [\mu(TS) - \mu(R)]$ and the activation hardness,[29] $\Delta\eta^{\neq} = [\eta(TS) - \eta(R)]$. These activation values are defined simply as the difference between the TS property and that which corresponds to the reactant (or intermediate) associated species. Furthermore, a Marcus-like equation can be used to rationalize the activation energy of simple processes[29,30]

$$\Delta V^{\neq} = V(\beta) = \left[\frac{1}{4}K_V + \frac{1}{2}\Delta V^0 + \frac{1}{4}\frac{(\Delta V^0)^2}{K_V}\right] \tag{5}$$

where K_V must be determined for each reaction and $\Delta V^0 = [V(P) - V(R)]$ is the energy difference between reactants and products. The position of the transition structure along a reduced reaction coordinate ω (0 for reactant, 1 for product), can be obtained through the Leffler's definition of the Brönsted coefficient (β)[30,31]

$$\beta = \frac{\partial \Delta V^{\neq}}{\partial \Delta V^0} \rightarrow \beta = \left[\frac{1}{2} + \frac{1}{2}\frac{\Delta V^0}{K_V}\right] \tag{6}$$

and provides a quantitative basis for the rationalization of the Hammond postulate.[32,33]

On the other hand, examination of local aspects of chemical reactivity can be done through the topological analysis of the electron localization function (ELF) of Becke and Edgecombe[13] introduced by Savin et al.[34,35] This methodological tool provides a nice convenient partition of the molecular space into basins of attractors, which can be interpreted consistently on the basis of chemical concepts of bonding such as atoms, bonds, lone pairs and finally, chemical structures.[36−38] Several interesting issues of chemical reactivity of stationary and reacting systems have been addressed with this increasingly useful tool.[39−44]

The $ELF(\mathbf{r})$ local function, is defined in terms of the excess of local kinetic energy density due to the Pauli repulsion, $T(\rho(\mathbf{r}))$, and the Thomas−Fermi kinetic energy density, $T_h(\rho(\mathbf{r}))$

$$ELF(\mathbf{r}) = \frac{1}{1 + \left[\frac{T(\mathbf{r})}{T_h(\mathbf{r})}\right]^2} \tag{7}$$

These quantities can be straightforwardly evaluated for a monodeterminantal wave function from the Hartree−Fock (HF) or the Kohn−Sham (KS) orbitals, $\varphi_i(\mathbf{r})$

$$T(\mathbf{r}) = \frac{1}{2}\sum_i |\nabla\varphi_i(\mathbf{r})|^2 - \frac{1}{8}\frac{|\nabla\rho(\mathbf{r})|^2}{\rho(\mathbf{r})} \tag{8}$$

$$T_h(\mathbf{r}) = 2.871\rho(\mathbf{r})^{5/3} \tag{9}$$

and

$$\rho(\mathbf{r}) = \sum_i |\varphi_i(\mathbf{r})|^2 \tag{10}$$

The gradient field of the ELF provides us with basins of attractors (Ω_i) whose associated properties can be related to chemical bonding characteristics of systems such as the electron delocalization (or localization).[34,37−39]

The population of a basin, $\tilde{N}(\Omega_i)$, is defined as the integral of the one electron density $\rho(\mathbf{r})$ over the basin

$$\tilde{N}(\Omega_i) = \int_{\Omega_i} \rho(\mathbf{r})d\mathbf{r} \tag{11}$$

the population variance, $\sigma^2(\tilde{N}_i)$, is calculated in terms of the diagonal elements of the first ($\rho(\mathbf{r})$) and second order ($\pi(\mathbf{r}_1,\mathbf{r}_2)$) density matrixes

$$\sigma^2(\tilde{N}, \Omega) = \int_{\Omega_i} d\mathbf{r}_1 \int_{\Omega_i} d\mathbf{r}_2 \pi(\mathbf{r}_1, \mathbf{r}_2) + \tilde{N}(\Omega) - [\tilde{N}(\Omega)]^2 \tag{12}$$

from which the standard deviation $\sigma(\tilde{N}_i)$ can be obtained. Finally, the above quantities can be used to define the positive relative fluctuation $\lambda(\tilde{N}_i)$ as

$$\lambda(\Omega) = \frac{\sigma^2(\tilde{N},\Omega)}{\tilde{N}(\Omega)} \tag{13}$$

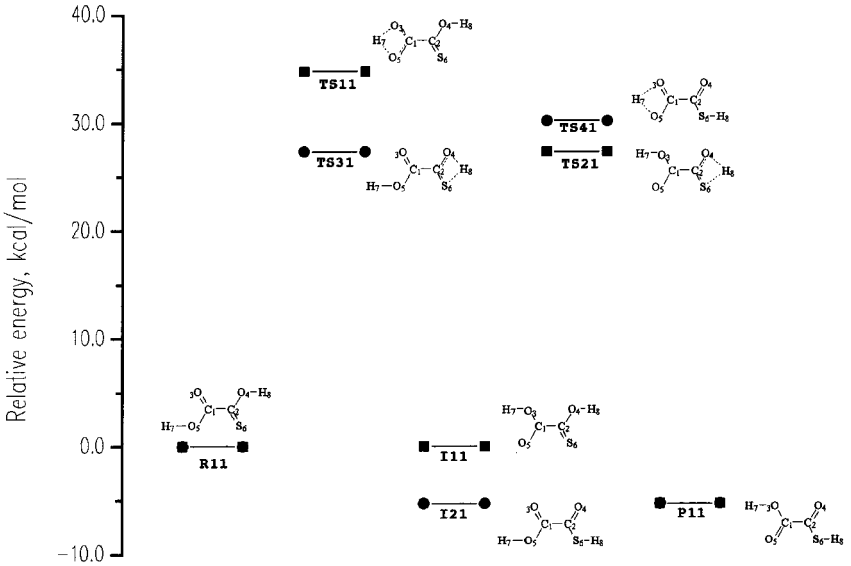

Figure 2. B3LYP/6-311+G(d,p) relative energy path for the double proton-transfer reactions in system (1). Square = Path 1, circle = Path 2.

These quantities are useful tools in the analysis of the electronic delocalization in several systems.[45] Comprehensive explanations concerning the methodology and nomenclature related to the topological analysis of ELF have been presented elsewhere by Savin et al.[34−38] In this context, the details of local electronic structure along the oxygen to oxygen, sulfur to oxygen, and sulfur to sulfur proton-transfer reactions in these systems have been addressed in this work.

Computational Details

All geometry optimizations have been carried out using the Gaussian 98 package of programs[46] within the Berny algorithm at the B3LYP/6-311+G(d,p) level. Twenty-four stationary points corresponding to the two step reaction mechanims for the three studied reactions were localized, optimized and finally characterized by the normal-mode analysis. Only one imaginary frequency has been found at the corresponding transition states. Global properties were calculated from optimized stationary points using eqs 1−6. The intrinsic reaction coordinate[47] was calculated to verify that the transition vectors connect, in each case, the corresponding reactant, intermediate and/or product species. The topological analysis of the electron localization function has been carried out using the TopMod package of programs,[48,49] which calculates the quantities in eqs 7−13 from the optimized wave function on a tridimensional grid surrounding the molecular system.[48,49]

Results and Discussion

Conformer interconversion with low-energy barriers have been previously observed for the parent oxalic acid compound.[50] It will be clear from our present results that such a type of interconversion in the thio-oxalic derivatives could also be an energetically efficient process and that several conformers with low energy-barriers may coexist. It will be also shown that a two step mechanism is more probable than a concerted double proton-transfer process in this series of thioxalic acid derivatives.

Global Aspects of Chemical Reactivity. An extensive search for the pathway 0 (Figure 1) of the potential energy surface corresponding to concerted reaction process via both TS0a or TS0b transition structures was carried out. Results show that a neutral concerted transition structure via five-membered transition structures such as TS0a is not possible for these thiooxalic derivatives because the valence requirements of the central carbon atoms along the interconversion path cannot be satisfied in any cases. On the other hand, the search for neutral concerted four-membered type transition structures such as TS0b in Figure 1, always converges to structures along the stepwise pathway 1 or pathway 2 at both the HF and the DFT levels of calculations.

TABLE 1: (a) Some Global Properties for Reaction 1 Obtained at the B3LYP/6-311+G(d,p) Level of Theory, (b) Activation and Reaction Parameters for Reactions (1) Calculated at the B3LYP/6-311+G(d,p) Level of Theory

(a) species	E_0, au	η, au	μ, au	$\langle\alpha\rangle$ au	NIMAG, i cm^{-1}
R11	−701.3516	0.0786	0.1839	55.56	NA
P11	−701.3601	0.0963	0.2001	53.57	NA
I11	−701.3516	0.0786	0.1839	55.56	NA
I21	−701.3601	0.0963	0.2001	53.57	NA
TS11	−701.2962	0.0875	0.1905	55.73	1963.3
TS21	−701.3081	0.0988	0.1927	54.62	1767.2
TS31	−701.3081	0.0987	0.1927	54.62	1767.5
TS41	−701.3035	0.0941	0.2153	53.37	1993.9

(b) step	$\Delta V^{\ddagger}$, kcal/mol	$\Delta\eta^{\ddagger}$, kcal/mol	$\Delta\mu^{\ddagger}$, kcal/mol	ΔV^0, kcal/mol	$\Delta\alpha^{\ddagger}$, au	$\Delta\alpha^0$, au	β
R11 → I11	34.8	5.6	4.1	0.0	0.2	0.00	0.50
I11 → P11	27.3	12.7	5.5	−6.5	−0.9	−2.4	0.47
R11 → I21	27.3	62.0	120.9	−5.3	−0.9	−2.0	0.47
I21 → P11	35.5	−1.4	9.5	0.0	−0.2	0.0	0.50

Figures 2−4 schematize all of the stationary points along the relative energy profile for the three reaction processes, including the numbering used in discussing the results. Optimized parameters for each point can be obtained as Supporting Information. Tables 1−3 report the total energy (zero-point energy corrected), global hardness η, chemical potential μ, mean polarizability $\langle\alpha\rangle$, and the imaginary normal frequency (for transition structures), corresponding to reactions 1, 2, and 3, respectively.

In Table 3b, we report the activation values of potential energy $\Delta V^{\ddagger}$, global hardness $\Delta\eta^{\ddagger}$, chemical potential $\Delta\mu^{\ddagger}$, and polarizability $\Delta\alpha^{\ddagger}$, as well as the energy ΔV^0, polarizability $\Delta\alpha^0$ reaction values, and the Brönsted coefficient β calculated using eqs 5 and 6.

Tables 4−9, report the basin populations (N_Ω), the variance σ^2, and the relative fluctuation values λ, for each optimized stationary point corresponding to the oxygen to oxygen (R11→TS11), sulfur to oxygen (R33→TS13), and sulfur to

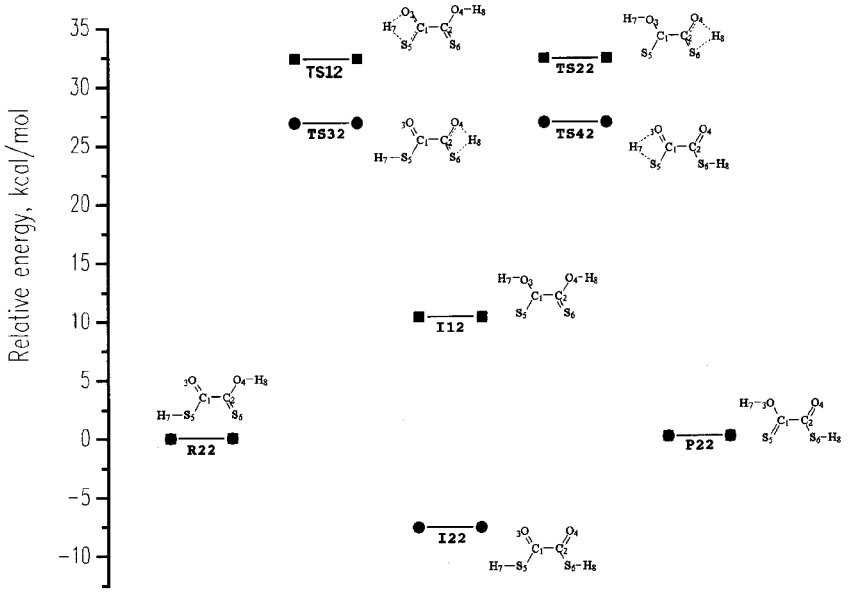

Figure 3. B3LYP/6-311+G(d,p) relative energy path for the double proton-transfer reactions in system (2). Square = Path 1, circle = Path 2.

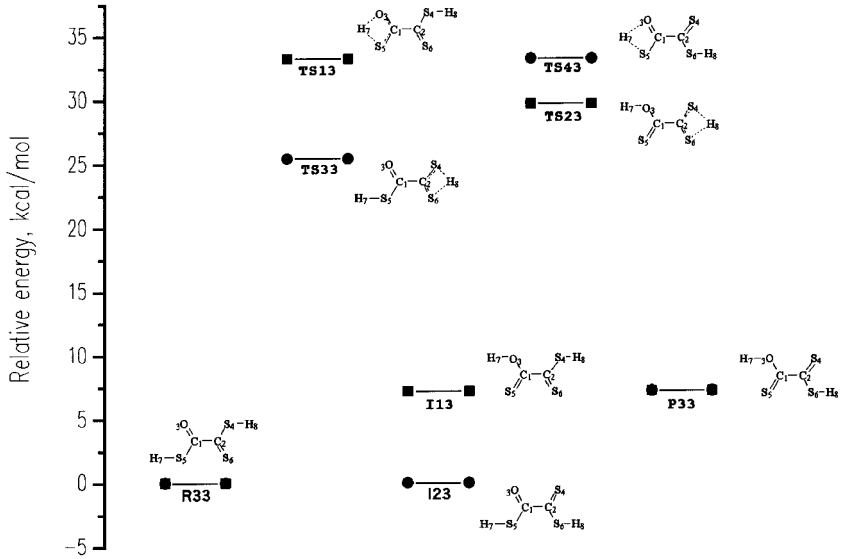

Figure 4. B3LYP/6-311+G(d,p) relative energy path for the double proton-transfer reactions in system (3). Square = Path 1, circle = Path 2.

sulfur (I13→TS43) proton transfer reactions. The core populations for C, O, and S are 2.1e, 2.1e, and 10.05e, respectively, and they are not included in these Tables. The absolute errors on the populations are at least 0.1e, and the difference in the core populations are not meaningful.

Monothiooxalic Acid Derivative (1). The monothioxalic derivative (1) implicate H(O) → O and H(O) → S proton-transfer reaction processes.

In pathway 1 of this process, the intermediate I11 is reached via the TS11 (O5 → O3 proton transfer) with an energetic barrier predicted in 34.8 kcal/mol. It can be noted that R11 and I11 are conformationally related species. The second step involves the O4 → S6 proton transfer via the TS21 with a energetic barrier of about 27.3 kcal/mol. The product, P11, is predicted to be 6.5 kcal/mol more stable than R11 (or I11). Through pathway 2, the TS31 (O4 → S6 proton transfer) connects with the I21 intermediate which is isoenergetic with P11. It is also noted that I21 and P11 are conformationally related species. The transition structure TS31 is located 7.5 kcal/mol below than the TS11 transition structure and the H(O) → S proton transfer result slightly favored respect to the H(O) → O one. The second step from I21 to P11 implies the O5 → O3 proton transfer with an activation energy of 30.2 kcal/mol. Thus, for the system

TABLE 2: (a) Some Global Properties for Reaction 2 Obtained at the B3LYP/6−311+G(d,p) Level of Theory (b) Activation and Reaction Parameters for Reactions (2) Calculated at the B3LYP/6−311+G(d,p) Level of Theory

(a) species	E_0, au	η, au	μ, au	$\langle\alpha\rangle$ au	IMAG, i cm^{-1}
R22	−1024.3124	0.0691	0.1963	70.66	NA
P22	−1024.3124	0.0691	0.1963	70.66	NA
I12	−1024.2960	0.0653	0.1862	76.32	NA
I22	−1024.3246	0.0843	0.1994	70.48	NA
TS12	−1024.2609	0.0686	0.2008	74.76	1789.8
TS22	−1024.2609	0.0686	0.2008	74.74	1789.8
TS32	−1024.2696	0.0794	0.2111	71.27	1818.1
TS42	−1024.2696	0.0794	0.2110	71.32	1818.3

(b) step	$\Delta V^{\ddagger}$, kcal/mol	$\Delta\eta^{\ddagger}$, kcal/mol	$\Delta\mu^{\ddagger}$, kcal/mol	ΔV^0, kcal/mol	$\Delta\alpha^{\ddagger}$, au	$\Delta\alpha^0$, au	β
R22 → I12	32.3	−0.4	2.8	10.3	4.1	5.7	0.55
I12 → P22	22.0	2.1	9.2	−10.3	−1.6	−5.7	0.45
R22 → I22	26.8	6.4	9.2	−7.6	0.6	−0.2	0.47
I22 → P22	34.5	−3.1	7.3	7.6	0.8	0.2	0.53

TABLE 3: (a) Global Properties for Reaction 3 Obtained at the B3LYP/6−311+G(d,p) Level of Theory (b) Activation and Reaction Parameters for Reactions (3) Calculated at the B3LYP/6−311+G(d,p) Level of Theory

(a) species	E_0, au	η, au	μ, au	$\langle\alpha\rangle$ au	IMAG, i cm^{-1}
R33	−1347.2811	0.0597	0.1966	87.75	NA
P33	−1347.2696	0.0569	0.1885	92.22	NA
I13	−1347.2696	0.0569	0.1885	92.22	NA
***I*23**	−1347.2811	0.0597	0.1966	87.75	NA
TS13	−1347.2281	0.0538	0.2026	89.09	1821.4
TS23	−1347.2337	0.0723	0.1856	93.12	1473.5
TS33	−1347.2406	0.0635	0.1993	89.05	1501.4
TS43	−1347.2281	0.0538	0.2026	89.40	1819.5

(b) step	ΔV^{π}, kcal/mol	$\Delta\eta^{\pi}$, kcal/mol	$\Delta\mu^{\pi}$, kcal/mol	ΔV^{0}, kcal/mol	$\Delta\alpha^{\pi}$, au	$\Delta\alpha^{0}$, au	β
R33 → I13	33.3	−3.7	3.7	7.2	1.3	4.5	0.53
I13 → P33	22.5	9.7	−1.8	0.0	0.9	0.0	0.50
R33 → *I*23	25.4	2.4	1.7	0.0	1.3	0.0	0.50
***I*23 → P33**	33.3	−3.7	3.7	7.2	1.7	4.5	0.53

TABLE 4: Topological ELF Properties for R11 at the B3LYP/6−311+G(d,p) Level of Theory

	basin, Ω	N_Ω	σ^2	λ
1	V(H7,O5)	1.74	0.80	0.46
2	V(H8,O4)	1.81	0.83	0.46
3	V(C1,C2)	2.27	1.06	0.47
4	V(C1,O3)	2.40	1.35	0.56
5	V(C2,S6)	2.64	1.38	0.52
6	V(C2,O4)	1.58	0.96	0.61
7	V(C1,O5)	1.62	0.98	0.60
8	$V_{1(O3)}$	2.50	1.16	0.46
9	$V_{2(O3)}$	2.63	1.20	0.45
10	V(O4)	4.13	1.46	0.35
11	V(O5)	4.24	1.47	0.35
12	V_1(S6)	2.52	1.16	0.46
13	$V_{2(S6)}$	2.64	1.20	0.45

TABLE 5: Topological ELF Properties for TS11 at the B3LYP/6−311+G(d,p) Level of Theory

	basin, Ω	N_Ω	σ^2	λ
1	V(H8,O4)	1.80	0.82	0.46
2	V(C1,O5)	3.54	1.72	0.49
3	V(C1,O3)	3.44	1.70	0.49
4	V(C1,C2)	2.25	1.05	0.47
5	V(C2,O4)	1.54	0.94	0.61
6	V(C2,S6)	2.65	1.39	0.52
7	V(H7)	0.52	0.42	0.80
8	V_1(O3)	3.32	1.35	0.41
9	$V_{2(O3)}$	0.37	0.32	0.87
10	V(O4)	4.14	1.46	0.35
11	$V_{1(O5)}$	3.08	1.30	0.42
12	$V_{2(O5)}$	0.46	0.39	0.84
13	$V_{1(S6)}$	2.66	1.21	0.45
14	$V_{2(S6)}$	2.47	1.16	0.47

TABLE 6: Topological ELF Properties for R33 at the B3LYP/6−311+G(d,p) Level of Theory

	basin, Ω	N_Ω	σ^2	λ
1	V(H7,S5)	1.81	0.71	0.39
2	V(H8,S4)	1.83	0.72	0.39
3	V(C1,C2)	2.17	1.06	0.49
4	V(C1,O3)	2.35	1.30	0.55
5	V(C1,S5)	1.89	1.06	0.56
6	V(C2,S6)	2.54	1.34	0.53
7	V(C2,S4)	1.88	1.06	0.56
8	$V_{1(O3)}$	2.63	1.19	0.45
9	$V_{2(O3)}$	2.38	1.14	0.48
10	$V_{1(S4)}$	2.00	1.01	0.50
11	$V_{2(S4)}$	2.03	1.02	0.50
12	$V_{1(S5)}$	2.10	1.04	0.49
13	$V_{2(S5)}$	2.06	1.03	0.50
14	$V_{1(S6)}$	2.49	1.17	0.47
15	$V_{2(S6)}$	2.58	1.17	0.45

TABLE 7: Topological ELF Properties for TS13 at the B3LYP/6−311+G(d,p) Level of Theory

	basin, Ω	N_Ω	σ^2	λ
1	V(H8,S4)	1.84	0.72	0.39
2	V(C1,C2)	2.21	1.07	0.48
3	V(C1,S5)	2.17	1.19	0.55
4	V(C1,O3)	1.92	1.13	0.59
5	V(C2,S6)	2.56	1.35	0.53
6	V(C2,S4)	1.89	1.06	0.56
7	V(H7)	0.58	0.45	0.77
8	$V_{1(O3)}$	3.59	1.43	0.40
9	$V_{2(O3)}$	1.59	0.94	0.59
10	$V_{1(S4)}$	2.01	1.01	0.50
11	$V_{2(S4)}$	2.03	1.01	0.50
12	$V_{1(S5)}$	3.93	1.53	0.39
13	$V_{2(S5)}$	1.37	0.84	0.61
14	$V_{1(S6)}$	2.51	1.13	0.45
15	$V_{2(S6)}$	2.53	1.17	0.46

TABLE 8: Topological ELF Properties for I13 at the B3LYP/6−311+G(d,p) Level of Theory

	basin, Ω	N_Ω	σ^2	λ
1	V(H8,S4)	1.88	0.71	0.38
2	V(H7,O3)	1.81	0.83	0.46
3	V(C1,C2)	2.19	1.07	0.49
4	V(C1,O3)	1.60	0.97	0.61
5	V(C1,S5)	2.56	1.35	0.53
6	V(C2,S4)	1.87	1.06	0.57
7	V(C2,S6)	2.54	1.35	0.53
8	V(O3)	4.12	1.47	0.36
9	$V_{1(S4)}$	2.09	1.02	0.49
10	$V_{2(S4)}$	1.99	1.02	0.51
11	$V_{1(S5)}$	2.67	1.22	0.46
12	V_2(S5)	2.50	1.18	0.47
13	$V_{1(S6)}$	2.49	1.15	0.46
14	$V_{2(S6)}$	2.58	1.18	0.46

(1) both pathways are a very close. Furthermore, proton-transfer reaction processes are coupled with rotational changes through the C−C bond, and therefore, the more probable interconversion will involve the conformational change of R11 into I11 followed by a single proton-transfer reaction from O4 to S6 (27.3 kcal/mol) yields the P11 product, which is also related to I21.

As can be seen from Table 1b, the position of the transition states along the reduced coordinate are 0.50, 0.47, 0.47, and 0.50 for TS11 (R11 → I11), TS21 (I11 → P11), TS31 (R11 → I21), and TS41 (I21 → P11), respectively. These predictions agree with what is expected from the Hammond postulate for the above-described energetic processes. It can be noted, however, from Table 1a that in the first symmetrical transfer proton reaction (O5 → O3) a global maximum hardness principle (MHP) does not hold (R11 hardness is predicted lower than TS11 and TS31 values), however the correct MHP relationship is predicted between all TSs species, being the more stable the harder one. The general observations concerning the hardness values agree with recent explanations of such a type of global analysis and its relation with the MHP in terms of the symmetry of the reaction process.[51]

1,2-Dithiooxalic Acid Derivative (2). This stepwise reaction mechanism implies H(S) → O and H(O) → S proton-transfer processes.

We can immediately note from the symmetry of the systems in (2) that R22 and P22 are essentially the same species. From Table 2a, we can see that the two-step mechanism for proton reaction processes through pathway 1 has activation barriers of 32.3 and 22.0 kcal/mol via the TS12 (S5 → O3) and TS22 (O4 → S6) transition structures, respectively. The I12 intermediate

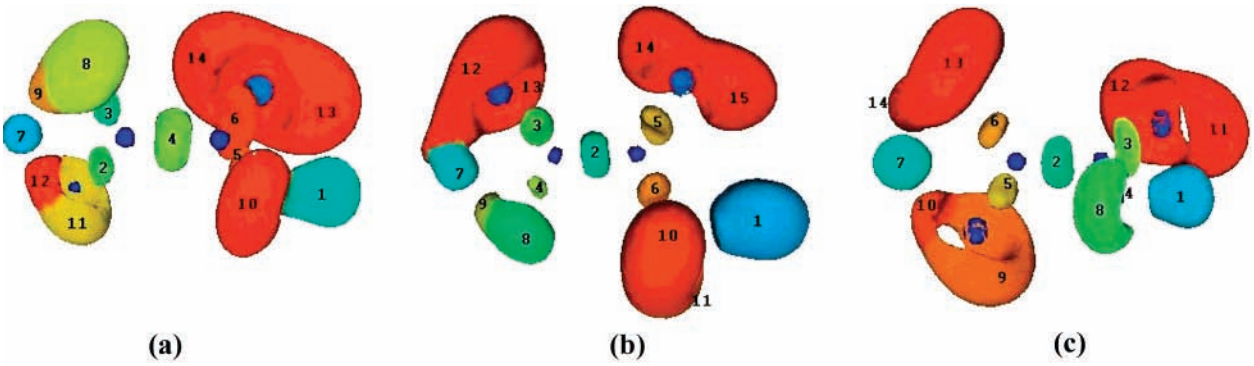

Figure 5. Localization basin domains represented for ELF = 0.75 from the optimized wave function at the B3LYP/6-311+G(d,p) level of theory for (a) TS11 [H(O5)→O3 proton transfer], (b) TS13 [H(S5)→O3 proton transfer], and (c) TS23 [H(S4)→S6 proton transfer]. Each basin has been identified by a different color. Numbering in each graph (a), (b), and (c), corresponds to the basin numeration in Tables 5, 7, and 9, respectively.

TABLE 9: Topological ELF Properties for TS23 at the B3LYP/6−311+G(d,p) Level of Theory

	basin, Ω	N_Ω	σ^2	λ
1	V(H7,O3)	1.84	0.84	0.46
2	V(C1,C2)	2.19	1.06	0.48
3	V(C1,S5)	2.58	1.36	0.53
4	V(C1,O3)	1.52	0.94	0.62
5	V(C2,S4)	2.16	1.19	0.55
6	V(C2,S6)	2.17	1.20	0.55
7	V(H8)	0.82	0.56	0.68
8	V(O3)	4.15	1.46	0.35
9	$V_{1(S4)}$	3.82	1.51	0.40
10	$V_{2(S4)}$	1.35	0.85	0.63
11	$V_{1(S5)}$	2.69	1.22	0.45
12	$V_{2(S5)}$	2.46	1.18	0.48
13	$V_{1(S6)}$	3.81	1.51	0.40
14	$V_{2(S6)}$	1.35	0.85	0.63

is located 10.3 kcal/mol above R22. In pathway 2, the relative activation energies have been determined to be 26.8 kcal/mol via the TS32 (O4 → S6) transition structure and 34.5 kcal/mol via the TS42 (S5 → O3) transition structure. The I22 intermediate is located 7.6 kcal/mol below R22. From Table 2b, the β values for TS12, TS22, TS32, and TS42 are 0.55, 0.45, 0.47, and 0.53, respectively. They are completely consistent with the Hammond postulate for the energy profile of this reaction. In these reactions, there is no symmetrical process along the single proton transfer reactions, and the hardness values cannot be related directly with the MHP. The H(O) → S processes are favored energetically by ∼5.0 kcal/mol in both pathways, corresponding to the lowest energy species with the highest hardness valued ones.

Trithio-Oxalic Acid Derivative (3). The reaction 3 comprises H(S) → O and H(S) → S proton-transfer reactions. In the pathway 1, activation energies of 33.3 kcal/mol (S5→O3 proton transfer) and 22.5 kcal/mol (S4→S6 proton transfer) are implicated in the transformations R33 → TS13 → I13 → TS23 → P33. The pathway 2, R33 → TS33 → *I*23 → TS43 → P33 involves activation barriers of 25.4 kcal/mol (S4→S6 proton transfer) and 33.3 kcal/mol (S4→S6 proton transfer). The intermediate I13 (which is conformationally related to P33), is located 7.2 kca/mol above of R33 (related conformationally to *I*23). Again, the β values associated with the TS13 (0.53), TS23 (0.50), TS33 (0.50), and TS43 (0.53) are consistent with the energetic description of both pathways in terms of the Hammond postulate. We observe that from the activation hardness values, the PMH is satisfied only in the case of S → O process, whereas it does not work for the S → S process (which is 7.9 kcal/mol favored in the overall process). The MPP on the other hand is satisfied in all cases for this reaction.

From Tables 1b, 2b, and 3b, we can note that relative activation energies for the proton-transfer reactions are estimated around 38.0 kcal/mol, 27.0, 33.0, and 25.0 kcal/mol for the O → O, O → S, S → O, and S → S, proton-transfer reactions, respectively. This observation agrees with the different degree of polarization character of oxygen and sulfur centers.

Conformational Changes through the C_1-C_2 Single Bond. In these three systems, the theoretical results point out that the proton-transfer reactions are coupled with rotational changes through the C1−C2 bond. For example, looking at the stationary points for reaction 1, the S6−C2−C1−O3 dihedral angle is 126.4°, 89.1°, 51.7°, 109.7°, and 179.9° for R1, TS11, I11, TS21, and P11, respectively, in the path1, and it is 126.4°, 70.8°, 180.0°, 180.0°, and 180.0° for R11, TS31, I21, TS41, and P11, respectively along the pathway 2. Migration of the H atom is concerted with the rotation through the C−C bond. Such rotation is related, as will be noted below from the local ELF analysis, with a more favorable charge rearrangement between the heterocenters along the interconversion path. For reactions 2 and 3, the accompanying rotational changes are also very pronounced. Thus, the mentioned dihedral angle is 180.0°, 36.9°, 48.6°, 37.4°, and 180.0° and 180.0°, 0.0°, 0.0°, 0.0°, and 180.0°, for the species involved in path1 and path 2 of reaction 2, respectively. The corresponding values in the case of reaction 3 are 180.0°, 180.0°, 41.5°, 0.0°, and 180.0°, 39.6°, 0.0°, 90.0°, 139.9°. At the present level of calculation, conformational barriers separating R11 and I11, I21 and P11, R33 and *I*23, I13 and P33 have been estimated to be only 2.3, 2.5, 2.4, and 3.0 kcal/mol, respectively. It is also clear that frontier orbital energies have changed not only because of the electronic and nuclear rearrangement resulting from the H transfer itself, but also as result of the global nuclear rearrangements along the total interconversion pathways. Therefore, we cannot expect that MPH and MPP are satisfied in all cases, as it has been observed from the respective activation values in Tables 1b-3b.

Local Aspects of Reactivity from the Topological Analysis of the ELF. With the aim to study in more detail the electronic nature of H(O) → O, H(S) → O, and H(S) → S proton-transfer reactions, we have analyzed the properties of the basins resulting from the topological analysis of the ELF in some representative transformations in these systems, specifically: (a) R11 → TS11, (b) R33 → TS13, and (c) I13 → TS23. Main results from eqs 7−13 are presented in Tables 4−9. Basin populations (N_Ω), the variance σ^2, and the relative fluctuation values λ, data in each case have been included. ELF pictures for the TSs are presented in Figure 5.

Ground States: R11, R33, I13. The delocalized electronic nature of the ground state species R11, R33, and I13, are clearly

emphasized from the structure and population properties of the ELF basins. In the case of R11, there are six core attractors corresponding to the C1, C2, O3, O4, O5, and S6 atomic centers. There are two protonated disynaptic basins associated with the O5−H7 and O4−H8 single bonds with populations of 1.74e and 1.81e, respectively, with medium values of delocalization ($\lambda = 0.46$). Monosynaptic valence basins associated with the valence pairs of the heteroatoms appears with populations of 2.50e, and 2.63e for O3, 4.24e for O5, 4.13e for O4 and 2.52e and 2.64e for S6, showing medium values of delocalization ($\lambda = 0.35-0.46$). The valence disynaptic V(C1,C2) basin carries 2.27e, whereas the double bonds between C1═O3 and C2═S6 (in a Lewis representation of bonding) appears with only 2.40e and 2.64e, respectively. At the other hand, the disynaptic valence basins associated with the C1−O5 and C2−O4 single bonds carry lowered populations of 1.62e and 1.58e which are highly delocalized ($\lambda = 0.60$). This picture of the R11 reactant species shows it as a polarized one along the S6−C2−C1−O3 chain. It is clearly noted the polarization effect of the O3 and S6 centers which contain 5.13e and 5.16e in their valence monosynaptic basins, respectively. Similar pictures can be drawn for the other ground-state species (R33 and I13) from data in Tables 6, and 8. In all these systems, the predicted localization agrees with our chemical intuition description of delocalization and polarization of the C−S and C−O bonds. It is clear that the known higher valence availability in the sulfur atoms is explicitly manifested from the properties of their monosynaptic and disynaptic related valence basins.

Transition Structures: TS11, TS13, TS23. In the reaction a, the TS11 transition structure associated with the transfer of H7 from O5 to O3, appears with a slightly asymmetric structure. This is not surprinsingly from the optimized structural data where the planes formed by the C1−O3−H7−O5, and C2−O4−H8−S6 are almost perpendicular, as noted above, and the stereochemical planes where the proton transfer occurs are not equivalent. From the analysis of data in Table 5, we have a monosynaptic protonated basin associated at the position of the H7, the transferred center, which contains only 0.52e. This population has associated a high delocalization value (0.80). There is not present any disynaptic basin associated with this center and therefore an ion-pair-like structure can be suggested for this transition state. A charge separation of 0.45e can be estimated for this structure. The population associated with the nonbonding pairs on the O3 and O5 atoms appears divided on two distorted and separated basins with asymmetric populations of 0.37e and 3.32e and 0.84e and 3.08e, respectively. These populations have high values of delocalization and can be rationalized as a distortion of the nonbonding pairs on the oxygen centers as the reaction proceed. Indeed, we can note from Table 5 that the charge on the remaining fragment is delocalized along the S6−C2−C1−O3 moiety. Stabilizing polarization is evident toward the terminal O3, O5, and S6 centers in this transition state structure.

In the case of the S5 → O3 proton transfer, reaction b, we can see from the analysis of Table 7 that an ion-pair like structure can be associated with the transition structure. The monosynaptic protonated basin V(H7) localizes only 0.58e implicating a total charge separation of 0.42e. The asymmetric structure for this transition state is reflected in the observed monsynaptic and disynaptic basin populations implicated in the H7−O3−C1−S5 four-membered cycle at TS13. Nonbonding population on the O3 and S5 are 5.18e and 5.30e, respectively. They are split and distorted as in the case of reaction a. Charge delocalization is evident now along the S6−C2−C1−S5 fragment and stabilizing polarization of negatively charged moiety occurs at terminal O3, S5, and S6 centers.

Finally, for the S4 → S6 proton transfer (H8) in reaction c, Table 9 shows similar characteristics but now the charge separation is only 0.18e in agreement with the electronegativity and greater polarizability of the sulfur centers. We can see that the structure is in contrast more symmetric. This fact implies that the S → S proton transfer is not very much affected by the substituents attached in the adjacent carbon atom, as is the case of H(O) → O transfer reaction described in (a). The monosynaptic protonated H8 basin localize 0.82e and the nonbonding population on the S5, S4, and S6 are 5.13e, 5.17e, and 5.17e indicating the stabilizing polarization of this structure.

Direct comparisons of the ELF results concerning the TS11, TS13, and TS23 transition structures, clearly manifiest the greater polarization character of the structure under introduction of the sulfur atoms. The abnormally higher populations of the V(C1,O3) and V(C1,O5) in TS11 compared to those of V(C1,-O3) and V(C1,S5) in TS13 can be rationalized again in terms of the better polarization of the nonbonding density on the S atom respect to the oxygen center. We note that there is a conjugative effect between the O and S nonbonding electrons, which is better emphasized when these populations are compared along the series of TSs. Thus we observe that the V(S5) in TS13 carries 5.16e, whereas the V(O5) in the case of TS11 counts for 3.54e.

Concluding Remarks

The intramolecular proton reactions in three different type of oxalic and thiooxalic acid derivatives, (1) HY−C(═O)−C(═S)−XH, X═O, Y═O; (2) X═O, Y═S; (3) X═S, Y═S, have been characterized from a theoretical viewpoint. A single concerted mechanism cannot be localized on the B3LYP/6-311+G(d,p) potential energy surface but only two-step processes are predicted. Four-membered transitions states are involved along the H(O) → O, H(S) → O, and H(S) → S single proton-transfer processes and the reactions are competitive and coupled with conformational rearrangements through the central single C−C bond in these systems. Thus, overall reaction energies implicated in the double proton transfer reactions are estimated in 65.7 kcal/mol, (62.8 kcal/mol), 54.3 kcal/mol (61.3 kcal/mol), and 55.8 kcal/mol (58.7 kcal/mol) for the reactions (1), (2), and (3), respectively, through the pathway 1 (pathway 2). Calculated values for the Brönsted coefficient are consistent with the Hammond postulate for the energy profile of these reactions. Finally, from the topological analysis of the electron localization function (ELF), we can observe explicitly the protonic nature of the transferred hydrogen atom. Only monosynaptic protonated valence basins are associated to the migrating center with total electron populations for the H(O) → O, H(S) → O, and H(S) → S proton-transfer reactions of 0.52e, 0.58e, and 0.82e, respectively. This observation agree and can be rationalized in terms of the greater polarizability introduced by the sulfur atoms. It can be though that a ion-pair like transition structures with charge separations of 0.48e, 0.42e, and 0.18e are implicated in these systems for the H(O) → O, H(S) → O, and H(S) → S single proton-transfer proton-transfer reactions, respectively.

Acknowledgment. This work has been supported by Catedra Presidencial en Ciencias awarded to A.T.L. and Fondecyt (Fondo Nacional de Desarrollo Científico y Tecnológico, Chile), Grant Nos. 2990030, 1990543, and 1010649. E. C. thanks also to Universidad de Chile-Mecesup through Grant No. UCH0008.

Supporting Information Available: All the 24 optimized geometries at the B3LYP/6-311+G(d,p), which corresponds to

both studied pathways for reactions 1, 2, and 3, have been included in the Gaussian Z-Matrix format. This material is available free of charge via the Internet at http://pubs.acs.org.

References and Notes

(1) Melander, L.; Saunders, W. H. J. *Reaction Rates of Isotopic Molecules*; John Wiley & Sons: New York, 1980.
(2) Jeffrey, G. A.; Saenger, W. *Hydrogen-Bonding in Biological Structures*; Springer-Verlag: Berlin, 1991.
(3) Scheiner, S. *Hydrogen Bonding*: *A Theoretical Perspective*; Oxford University Press: New York, 1997.
(4) Eigen, M. *Angew Chem. Int. Ed. Engl.* **1964**, *3*, 1.
(5) Brzezinski, P. *Biochim. Biophys. Acta* **2000**, *1458*, 1.
(6) Krishtalik, L. I. *Biochim. Biophys. Acta* **2000**, *1458*, 6.
(7) Dietzch, W.; Strauch, P.; Hoyer E *Coord. Chem. Rev*., **1992**, *21*, 43.
(8) Thiel, W.; Mayer, R. *Sulfur Rep*., **1988**, *8*, 1.
(9) Jeroschwski, P.; Hansen, P. *Sulfur Rep*. **1986**, *7*, 1.
(10) Remko, M.; Smiesko M.; Van-Duijnen P. T. *Mol. Phys.* **2000**, *98*, 709.
(11) Remko, M.; Liedl, K. R.; Rode, B. M. *J. Mol. Struct. (THEOCHEM)* **1997**, *418*, 179.
(12) Remko, M.; Liedl, K. R.; Rode, B. M. *Chem. Phys. Lett*. **1996**, *263*, 379.
(13) Becke, A. D.; Edgecombe, K. E. *J. Chem. Phys.* **1990**, *92*, 5397.
(14) Parr R. G., and W. Yang, *Density Functional Theory of Atoms and Molecules*; Oxford University Press: New York, 1989.
(15) Parr, R. G.; Donnelly, R. A.; Levy, M.; Palke, W. E., *J. Chem. Phys*. **1978**, *68*, 3801.
(16) Perdew, J. P.; Parr, R. G.; Levy, M.; Balduz, J. L. *Phys. Rev. Lett*. **1982**, *49*, 1691.
(17) Parr, R. G.; Pearson, R. G. *J. Am. Chem. Soc*. **1983**, *105*, 7512.
(18) Yang, W.; Parr, R. G. *Proc. Natl. Acad Sci. U. S. A*., **1983**, *82*, 6723.
(19) Pearson, R. G. *Chemical Hardness: Applications from Molecules and Solids*; Wiley-VCH Verlag GMBH: Weinheim, Germany, 1997.
(20) Chattaraj, P. K.; Sengupta, S. *J. Phys. Chem*. **1996**, *100*, 16 126.
(21) Pearson, R. G. *J. Chem. Educ*. **1987**, *64*, 561.
(22) Parr, R. G.; Chattaraj, P. K. *J. Am. Chem. Soc*. **1991**, *113*, 1854.
(23) Pearson, R. G. *Acc. Chem. Res.* **1993**, *26*, 250.
(24) Chattaraj, P. K. *Proc. Indian Natl. Sci. Acad − Part A* **1996**, *62*, 1133.
(25) Ayers, P. W.; Parr, R. G. *J. Am. Chem. Soc*. **2000**, *122*, 2010.
(26) Chattaraj, P. K.; Liu, G. H.; Parr, R. G. *Chem. Phys. Lett*. **1995**, *237*, 171
(27) Sadlej, A. J. *Collect Czech. Chem. Commun.* **1995**, *53*, 1988.
(28) Basis sets were obtained from the *Extensible Computational Chemistry Environment Basis Set Database*, as developed and distributed by the Molecular Science Computing Facility, Environmental and Molecular Sciences Laboratory which is part of the Pacific Northwest Laboratory, P.O. Box 999, Richland, WA 99352, USA, and funded by the U.S. Department of Energy. The Pacific Northwest Laboratory is a multi-program laboratory operated by Battelle Memorial Institue for the U.S. Department of Energy under contract DE-AC06−76RLO 1830. Contact David Feller or Karen Schuchardt for further information.
(29) Pérez, P.; Toro-Labbe, A. *J. Phys. Chem A*., **2000**, *104*, 1557.
(30) Toro-Labbe, A. *J. Phys. Chem. A*., **1999**, *103*, 4398.
(31) Leffler, J. E. *Science* **1953**, *117*, 340.
(32) Hammond, G. S. *J. Am. Chem. Soc*. **1955**, *77*, 334.
(33) Solá, M.; Toro-Labbé, A. *J. Phys. Chem. A*. **1999**, *103*, 8847.
(34) Savin, A.; Nesper, R.; Wengert, S.; Fäsler, T. F. *Angew. Chem. Int. Ed. Engl*. **1997**, *36*, 1808.
(35) Marx, D.; Savin, A. *Angew. Chem. Int. Ed. Engl*. **1997**, *36*, 2077.
(36) Kohout, M.; Savin, A. *J. Comp. Chem.* **1997**, *18*, 1431.
(37) Savin, A.; Silvi, B.; Colonna, F. *Can. J. Chem.* **1996**, *74*, 1088.
(38) Silvi, B.; Savin, A. *Nature (London)* **1994**, *371*, 683.
(39) Fuster, F.; Sevin, A.; Silvi, B. *J. Phys. Chem. A* **2000**, *104*, 852.
(40) Chevreau, H.; Sevin, A. *Chem. Phys. Lett.* **2000**, *322*, 9.
(41) Chattaraj, P. K.; Chamorro, E.; Fuentealba, P. *Chem. Phys. Lett.* **1999**, *314*, 114.
(42) Krokidis, X.; Golcalves V.; Savin, A.; Silvi, V. *J. Phys. Chem. A.* **1998**, *102*, 5065.
(43) Krokidis, X.; Vuilleumier, R.; Borgis, D.; Silvi, B. *Mol. Phys*. **1999**, *96*, 265.
(44) Chamorro, E.; Santos, J. C.; Gómez, B.; Contreras, R.; Fuentealba, P. *J. Chem. Phys.* **2001**, *114*, 23.
(45) Bader, R. F. W. *Localization and Delocalization in Quantum Chemistry*; Chalvet, O., et al., Eds.; Reidel: Dordrecht, 1976, Vol. 1.
(46) Frisch, M. J.; Trucks, G. W.; Schlegel, H. B. Scuseria, G. E.; Robb, M. A.; Cheeseman, J. R.; Zakrzewski, V. G.; Montgomery, Jr. J. A.; Stratmann, R. E.; Burant, J. C.; Dapprich, S.; Millam, J. M.; Daniels, A. D.; Kudin, K. N.; Strain, M. C.; Farkas, O.; Tomasi, J.; Barone, V.; Cossi, M.; Cammi, R.; Mennucci, B.; Pomelli, C.; Adamo, C.; Clifford, S.; Ochterski, J.; Petersson, G. A.; Ayala, P. Y.; Cui, Q.; Morokuma, K.; Malick, D. K.; Rabuck, A. D.; Raghavachari, K.; Foresman, J. B.; Cioslowski, J.; Ortiz, J. V.; Baboul, A. G.; Stefanov, B. B.; Liu, G.; Liashenko, A.; Piskorz, P.; Komaromi, I.; Gomperts, R.; Martin, R. L.; Fox, D. J.; Keith, T.; Al-Laham, M. A.; Peng, C. Y.; Nanayakkara, A.; Challacombe, M.; Gill, P. M. W.; Johnson, B.; Chen, W.; Wong, M. W.; Andres, J. L.; Gonzalez, C.; Head-Gordon, M.; Replogle, E. S.; Pople, J. A. *Gaussian 98*, *Revision A.9*, Gaussian, Inc.; Pittsburgh, PA, 1998.
(47) Gonzalez, C.; Schlegel, H. B. *J. Phys. Chem.* **1990**, *94*, 5523.
(48) Noury, S.; Krokidis, X.; Fuster F.; Silvi, B. *TopMoD Package*, Université Pierre et Marie Curie, 1997.
(49) Noury, S.; Krokidis, X.; Fuster, F.; Silvi, B. *Comp. Chem.* **1999**, *23*, 597.
(50) See, for example: Chen, C.; Shyu, S. *Int. J. Quantum Chem*. **2000**, *76*, 541; Godfrey, P. D.; Mirabella, M. J.; Brown, R. D. *J. Phys. Chem. A* **2000**, *104*, 258; Macoas, E. M. S.; Fausto, R.; Pettersson, M.; Khriachtchev, L.; Raesaenen, M. *J. Phys. Chem. A* **2000**, *104*, 6956.
(51) Chandra, A. K.; Uchimaru T. *J. Phys. Chem. A.* **2001**, *105*, 3578.